Synthesis of self-assembled Ge nanocrystals employing reactive RF sputtering

A. Hernández-Hernández[a], L.A. Hernández-Hernández[b], B. Marel Monroy[c], J. Santoyo-Salazar[d], G. Santana-Rodríguez[c], A. Márquez-Herrera[e], S. Gallardo-Hernández[d], P.G. Mani-González[f] and M. Meléndez-Lira[g,*]

[a]*Escuela Superior de Apan, Universidad Autónoma del Estado de Hidalgo, Calle Ejido de Chimalpa Tlalayote s/n Colonia Chimalpa, Apan Hidalgo, México.*

[b]*Escuela Superior de Física y Matemáticas del Instituto Politécnico Nacional, Edificio 9 U.P. Adolfo López Mateos, Col. San Pedro Zacatenco, 07730 CDMX, México.*

[c]*Instituto de Investigaciones en Materiales, Universidad Nacional Autónoma de México, Apartado Postal 70-360, Coyoacán, 04510, CDMX, México.*

[d]*Departamento de Física, Centro de Investigación y de Estudios Avanzados del Instituto Politécnico Nacional, Apartado Postal 14740, CDMX, 07300, México.*

[e]*Departamento de Ingeniería Agrícola, DICIVA, Campus Irapuato-Salamanca, Universidad de Guanajuato, Ex Hacienda el Copal km 9, Carr. Irapuato-Silao, Irapuato, Gto 36500 México.*

[f]*Instituto de Ingeniería y Tecnología, Departamento de Física y Matemáticas, Universidad Autónoma de Ciudad Juárez, Chihuahua, México.*

[g]*Instituto de Ingeniería y Tecnología, Departamento de Física y Matemáticas, Universidad Autónoma de Ciudad Juárez, Chihuahua, México.*

Received 11 December 2015; accepted 30 June 2016

This work presents the results of a simple methodology able to control crystal size, dispersion and spatial distribution of germanium nanocrystals (Ge-NCs). It takes advantage of a self-assembled process taken place during the deposit of the system SiO_2/Ge/SiO_2 by reactive RF sputtering. Nanoparticles formation is controlled mainly by the roughness of the first SiO_2 layer but the ulterior interaction of the interlayer with the top layer also play a role. Structural quality of germanium nanocrystals increases with roughness and the interlayer thickness. The tetragonal phase of germanium is produced and its crystallographic quality improves with interlayer thickness and oxygen partial pressure. Room temperature photoluminescence emission without a post growth thermal annealing process indicates that our methodology produces a low density of non-radiative traps.

Keywords: Nanocrystals; reactive RF sputtering; germanium; heteroestructure.

PACS: 68.65.Hb; 68.65.Ac; 81.16.Dn

1. Introduction

Even when semiconductor science had a strong development when high purity crystals of germanium were produced the technological application of germanium was hindered because the lack of a native oxide adequate for device fabrication [1]. However taking advantage of its high intrinsic mobility and silicon compatibility the fabrication and technological application of heterojunction bipolar transistors have been successful implemented and the research of new of germanium based devices actively pursued [2]. Besides of the research for a direct application of germanium layers in the production of electronic devices there is interest in to employ it as buffer layer for the integration of the matures silicon-based electronics and III-V optoelectronics technologies [3-4]. As for any other material the promise of the nanotechnology revolution has arouse a huge interest for the production of Ge nanoparticles. The potential for applications of the nanoparticles depend on the specific characterists of materials. There are semiconductor nanoparticles with potential as biological markers [5-7], in the manufacture of storage devices [8-10], light emission and detection [11-13] or fabrication of optoelectronic and photovoltaic devices [14]. Nanoparticles production has been carried out employing different film growth techniques such as molecular beam epitaxy, metal organic chemical vapor deposition and sputtering; in general the growth mechanism of the nanoparticles is the production of islands through the Stranski-Krastanov mechanism trying to optimize the control on the size and spatial distribution of nanocrystals [15,16].

As a semiconductor of the IV group germanium is easily compatible with the dominant silicon technology and because its band gap and dielectric properties the synthesis of germanium nanoparticles is interesting for applications in photovoltaics [17], charge storage [18] and also as improving element in thin film capacitors [19]. There are several approaches for the production of germanium nanoparticles but because of the interest of this work we just mention some of those using Ge nanoparticles embedded within SiO_2 films. The methods that have been suggested employ direct ion implantation of Ge in SiO_2 films and sputtering modifications using germanium pieces glued on a silicion target or separated targets of SiO_2 and Ge [20,21]; however those methods have the disadvantage of requiring an additional thermal annealing process to promote germanium nucleation to the formation of nanoparticles. Our approach allows the growth of self-assembled germanium nanoparticles employing a sequential deposition of SiO_2/Ge/SiO_2 layers using the rough-

TABLE I. Growth conditions for three groups of samples.

Ge thickness	OPP 25% Sample	OPP33% Sample	OPP50% Sample	OPP66% Sample	OPP75% Sample
∼2.3 nm	OPPGe25Th23	OPPGe33Th23	OPPGe50Th23	OPPGe66Th23	OPPGe75Th23
∼4.7 nm	OPPGe25Th47	OPPGe33Th47	OPPGe50Th47	OPPGe66Th47	OPPGe75Th47
∼7.2 nm	OPPGe25Th72	OPPGe33Th72	OPPGe50Th72	OPPGe66Th72	OPPGe75Th72

ness of the first SiO_2 layer, produced due to the parameters employed during the sputtering process, as a template for the Ge-NCs. This methodology, reported in previous works, is employed here to shown the capability to control crystal size, dispersion and spatial distribution of self-assembled germanium nanocrystals (Ge-NCs) through the thickness of the germanium layer in the structure SiO_2/Ge/SiO_2 [11,22]. The reported results shown as the employed growth conditions allow the control of the crystalline phase, size and spatial distribution of the self-assembled Ge-NCs.

2. Experimental details

A set of SiO_2/Ge/SiO_2 heterostructures were deposited sequentially employing RF sputtering. The deposition characteristics allowed the formation of self-assembled germanium nanocrystals embedded in a silicon oxide matrix. The SiO_2/Ge/SiO_2 heterolayers were grown at 400°C on p-type Si (1 1 1) substrates by the RF magnetron sputtering technique, employing polycrystalline silicon and germanium targets (both 99.999% pure). The heterostructures were grown as follows: initially a layer of SiO_2 was deposited, then a thin layer of Ge, and on top of it another SiO_2 layer. After the deposition of each layer the plasma was turned off and the chamber evacuated until a pressure around 2×10^{-6} Torr was reached. Roughness of the silicon oxide films was modulated employing the following oxygen partial pressure values (OPP = oxygen pressure/ oxygen pressure + argon pressure): 25%, 33%, 50%, 66% and 75%, during the sputtering process. The Ge layer was grown employing an Ar atmosphere. During the growth of the heterostructure total gas pressure in the chamber was kept constant at 20 mTorr. The thickness of the layers was controlled through the deposition time: 15 min for the deposition of each silicon oxide layer and 1, 2 and 3 min for the Ge interlayer. RF power applied to the silicon and the germanium targets was 100 W and 15 W, respectively. When the growth was finished, the samples were kept inside the system until room temperature was attained. The thickness of SiO_2/Ge/SiO_2 samples was around ~ 200 nm. The typical deposition rate for germanium thin layers grown at similar conditions (~ 0.04 nm/s) would give thicknesses around ~ 2.3 nm, 4.7 nm and 7.2 nm for the germanium interlayers, considering a linear rate deposition.

The surface topography for SiO_2 reference samples was carried out by atomic force microscopy (AFM), employing an Autoprobe CP Research microscope in contact mode. The infrared (IR) transmission spectra were obtained with a Nicolet 750 FTIR system. The crystallographic properties of the samples were studied by grazing incidence X-ray diffraction at 1.5 degrees carried out in a Siemens D5000 system employing the Cu Kα wavelength. Photoluminescence measurements were done employing a lock-in standard technique using a 275 M Acton single spectrometer equipped with a 1200 lines/mm grating blazed at 500 nm and a silicon photomultiplier as a detector; the width of both slits was set at 100 μm. The excitation source was a 473.8 nm diode pumped solid-state laser.

3. Results and discussion

Figure 1(a), shows AFM micrographs of representative samples from a SiO_2 thin film grown on the silicon substrate. It is assumed that those characteristics would be reproduced in the first layer of the heterostructure SiO_2/Ge/SiO_2. In Fig. 1(b) it is shown the root mean square roughness (RMS roughness) as a function of the OPP employed. Surface roughness acts as a template to promote the formation of Ge nanoparticles because of the natural germanium accumulation in the valleys and accelerated erosion on the hills of the surface. Also, as it will be shown, roughness modulates the size and distribution of nanoparticles. As expected the roughness increases with increasing OPP, which is related with re-sputtering processes on the SiO_2 thin layer due to the higher reactivity of the plasma [23]. Samples were organized in three sets using the interlayer germanium thickness as identifier, as shown in Table I.

Figure 2 shows X-ray diffraction (XRD) patterns of samples deposited employing the different germanium thicknesses grouped under OPPGe25, OPPGe50 and OPPGe75. Those from OPP30 and OPP66 are omitted because their similarity with OPP25 and OPP75 respectively. Because the employed methodology it is expected the presence of silicon and germanium related compounds. Thus diffraction peaks were indexed using powder diffraction files 040545 for cubic Ge (C-Ge), 1805749 for tetragonal Ge (T-Ge), 0271402 for cubic silicon (C-Si) and 361463 for hexagonal GeO_2.

For the whole set of samples, the presence of diffraction peaks associated to silicon and cubic germanium is observed. For germanium the most prominent is the corresponding to the plane (111) observed at 27° upon a broad structure associated to an amorphous contribution. The peaks observed at 45.3° and 53.7° correspond to the planes (2 2 0) and (3 1 1)

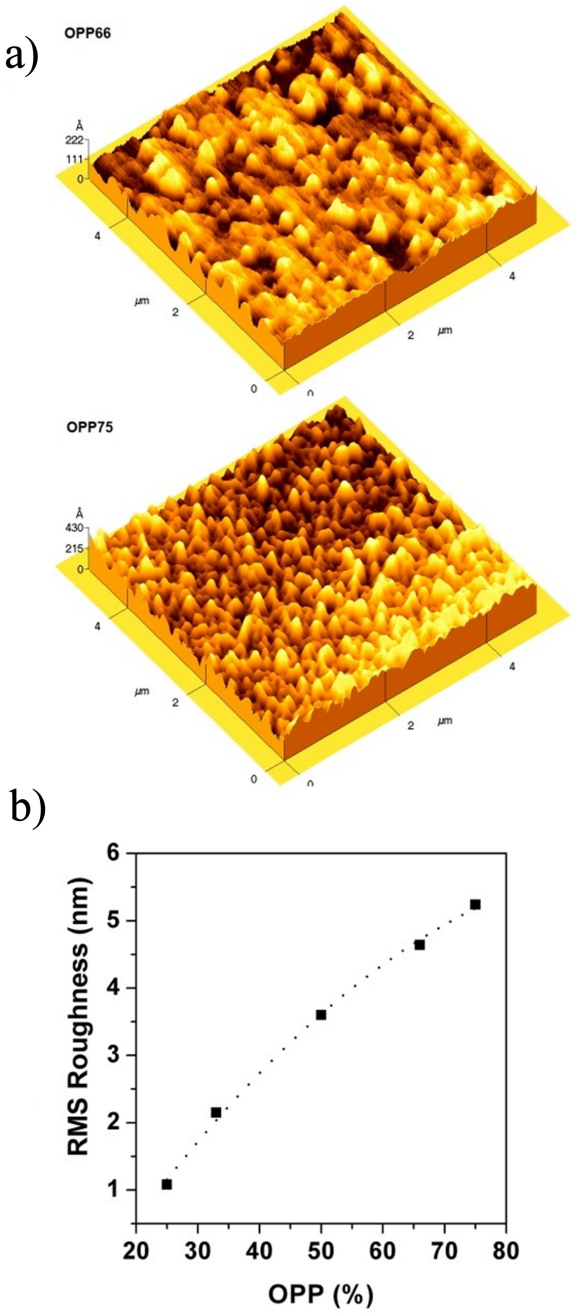

FIGURA 1. a) AFM micrographs of some representative SiO_2 reference samples: OPP66% and OPP75%. b) RMS roughness vs OPP graph.

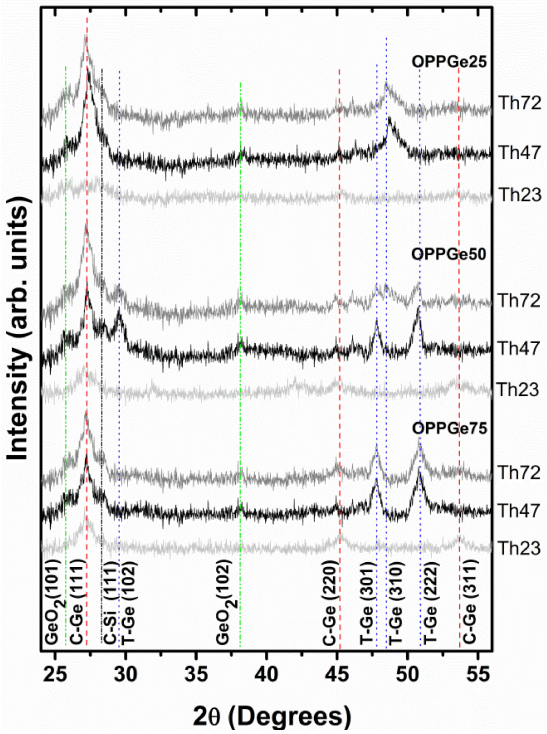

FIGURA 2. XRD of the SiO_2/Ge-NCs/SiO_2 samples at OPP25%, OPP50% and OPP75% for whole set of thicknesses of Ge interlayer. a) ∼2.3 nm (Th23), b) ∼4.7 nm (Th47) and c) ∼7.2 nm (Th72), respectively.

this phase. It is worth to note that the XRD patterns from samples with the thinnest germanium interlayer only show the presence of germanium cubic phase. The diffraction peaks located at 25.8° and 38° corresponding to the (1 0 1) and (1 0 2) diffraction planes of hexagonal GeO_2 respectively. The diffraction peaks observed at 48°, 29°, 47.5° and 51° are identified as diffractions from the planes (3 1 0), (1 0 2), (3 0 1) and (2 2 2) of tetragonal germanium. The presence of the tetragonal phase of germanium, reported as a high pressure phase, whose presence depends on the thickness of germanium interlayer adds an additional interest to our deposition methodology.

As the germanium interlayer thickness increases, the presence of contributions associated with the tetragonal germanium phase is evident in the XRD patterns indicating a higher formation of material with this crystallographic orientation. A close analysis of Fig. 2 shows that OPP also plays a role in the formation of the cubic or the tetragonal germanium phases; growth conditions at OPP50 could be associated to a transition point in the crystallographic characteristics of germanium nanocrystals. In Fig. 2 it is clear that as OPP increases the broad peak at 48° (OPPGe25) disappears giving place to slender peaks, located at 47.5° and 51°, indicating an increase in crystallographic quality. The fact that diffraction peak intensity is proportional to the amount of diffracted material allows establishing that the increase in crystalline quality and percentage of tetragonal phase is done to expenses of cubic germanium phase. It is supported with the results shown in Fig. 3 where the total area under the diffraction peaks of the cubic and the tetragonal phases are plotted. The increase of the area under the peaks associated with tetragonal phase as OPP increases is clearly observed. A first approximation to explain the presence of the tetragonal phase of germanium is to consider the behavior of the elastic properties of Ge and SiO_2 during the cooling process from 400°C to room temperature. However, since the germanium linear expansion coefficients is an order of magnitude larger than that of silicon oxide ($\alpha_{Ge} \sim 5.8 \times 10^{-6}$ °C^{-1} and

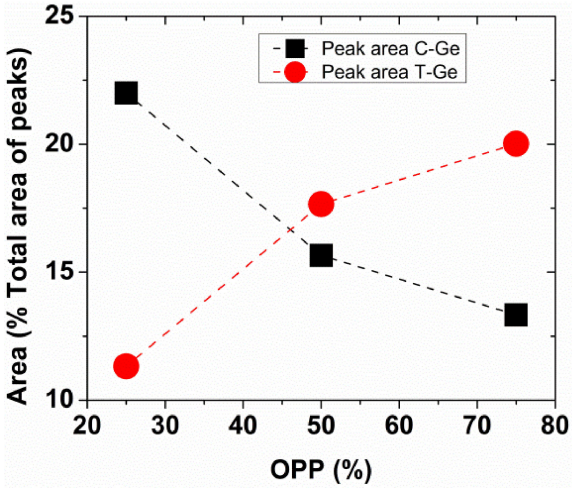

FIGURA 3. Graph OPP vs % Total area of the peaks. Comparison in proportion of the total sum of peaks areas of C-Ge and Ge-T.

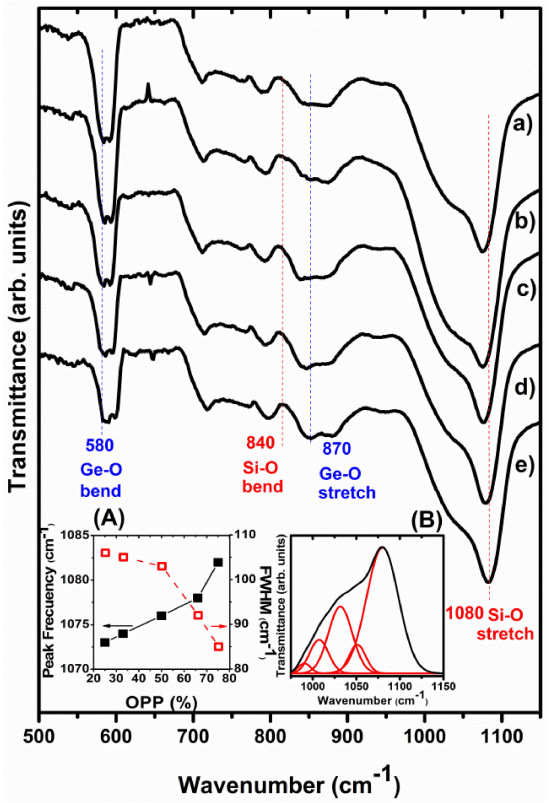

FIGURA 4. IR transmittance spectra of SiO_2/(Ge-NCs)/SiO_2 heteroestructure at different OPP: a)OPP25, b) OPP33, c) OPP50, d) OPP66 and e) OPP75). Inset A: Peak frequency and FWHM of the TO_3 vibrational mode at 1082 cm^{-1} vs OPP. Inset B: deconvolution of the 1082 cm^{-1} band into components.

and $\alpha_{SiO_2} \sim 5 \times 10^{-7}\ ^\circ C^{-1}$) the result is a tensile rather than compressive stress [24]. Then the formation of the tetragonal phase must be related with the reactive processes generated in the interface during the growth process. Germanium nanoparticles with tetragonal crystallographic orientation have been reported in several works [25]. Usually, it is suggested that an annealing process is responsible of its crystallographic characteristics. It is worth to mention that Jonnapoules *et al*. [26] have suggested that there could be a close relationship between electronic properties of amorphous germanium and its tetragonal phase, because of the similitude in short range order between them. On the other hand, the presence of high pressure phases can be expected theoretically in nanoclusters due to bond contractions [27].

The diffractograms presented in Fig. 2 allow stablishing an additional feature of the employed growth process: rougher surfaces produce nanocrystals with higher crystalline order. In order to obtain further information about the nanocrystals formed their vibrational properties were studied by infrared spectroscopy.

Figure 4 shows the IR transmittance spectra obtained for the SiO_2/Ge/SiO_2 heterostructures. All spectra show two well defined absorptions signals located at $\sim$840 and $\sim$1,080 cm^{-1}, associated with the bending [28] and asymmetric stretching vibration modes of Si-O-Si [29]. The presence from GeO_2 is established through the signals at around 580 and 870 cm^{-1}, associated with the Ge-O-Ge bending and stretching vibrational modes [30]. Even when some changes are observed in the above mentioned features it is difficult to extract additional information. Oxygen partial pressure controls surface roughness but it also affect the growth kinetics of germanium nanocrystals through the interaction with the SiO_2 layer. It is well established that the IR absorption feature located at $\sim$1082 cm^{-1} is directly related to the stoichiometry of silicon oxide [31], in Fig. 4 a shift in the minimum of this absorption band is clearly observed. As the OPP increases the width of the band diminishes and the position goes to the value associated to stoichiometric SiO_2. The inset a) in Fig. 4 summarizes the values for peak position and FWHM obtained by deconvolution of this absorption peak as shown in the inset b). The deconvolution process was carried out considering contributions from the transverse stretching vibration mode of the bridging oxygen atom in the Si-O_4 tetrahedra at 1058 cm^{-1} [32-34] and the Si-O-Si_3 and Si-O-Si_2 molecular clusters of low-oxidized silicon at 999 and 1030 cm^{-1} [35,36]. From the results shown in the inset of Fig. 4 it is clear that the heterostructures SiO_2/Ge/SiO_2 deposited at low OPP have silicon dioxide non-stoichiometric; giving place to oxygen-deficient diamagnetic defects. At this point it can be established that the studied heterostructures contain a mixture of SiO_2 and SiO_x phases with the SiO_x phase localized in the transition layers around germanium nanocrystals. It has been reported that the presence of germanium atoms promotes the oxidation of silicon [37]. It is plausible to expect that the redox reaction Si+GeO_2=Ge+SiO_2 occurs during the deposition process increasing the stoichiometry of SiO_2, reflected in the increase of vibrations associated with the Si-O_4 configuration. It is expected that the germanium interlayer deposited on top of the hills of the first SiO2 layer get strongly oxidized due to the reactive atmosphere giving place to a GeO_2 shell around the Ge-NCs and changing the stoichiometry of the adjacent

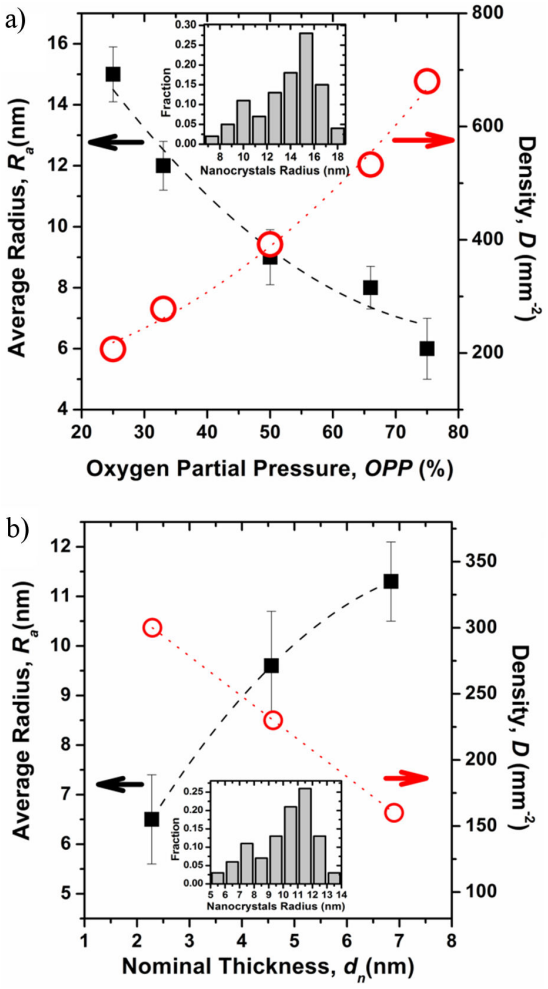

FIGURA 5. a) Average radius, Ra, and number density of Ge-NCs, D, plotted as a function of oxygen partial pressure in samples with same Ge intermediate thickness (∼4.7 nm). b) Average radius, R_a, and number density of Ge-NCs, D, plotted as a function of initial thickness dn. Insets, size distribution of Ge-NCs for a representative sample. This histogram show bimodal size distribution: large NCs with narrow distribution and small NCs with broad distribution.

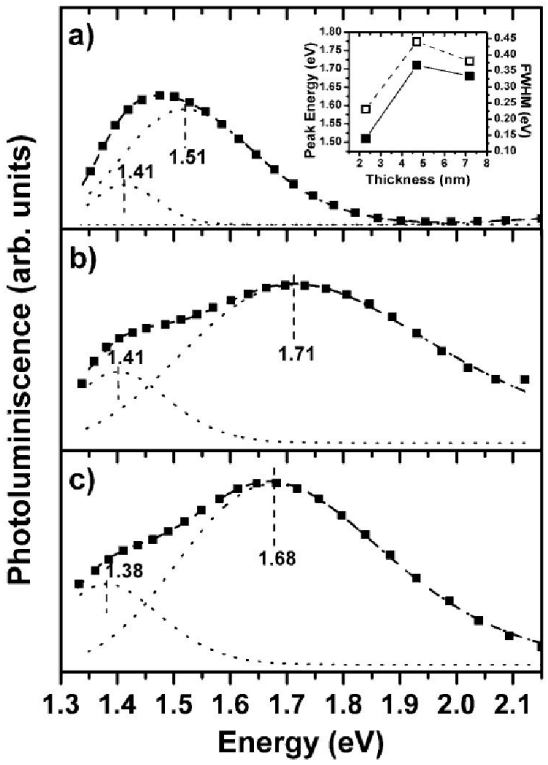

FIGURA 6. Room temperature photoluminescence spectra of samples grown at OPP75%. PL spectrums correspond to the sample with Ge interlayer thicknesses of : a) ∼2.3 nm, b) ∼4.7 nm and c) ∼7.2 nm, respectively. Experimental data are represented by dots, the Gaussian fittings by the broken lines. Continuous line represents the fitting to the experimental PL spectrum. Inset, correspond to graph of behavior of maximum PL peak as a function of thickness (black dots and continues line), and FWHM vs thickness (white dot and broken ine).

SiO_2 layer. The tetragonal phase of germanium is formed at this step due to the stress due to the formation of the different phases. When thin layers of germanium are deposited on SiO_2 layers with low roughness germanium is most exposed to the action of the reactive atmosphere giving place to greater amount of GeO_2 and through the interaction process with the adjacent layers to an increase in the non-stoichiometric SiO_2 phase. Then 2 nm could be established as a limit for the thickness of the Ge layer to grow Ge-NCs by this method.

The whole set of samples have been characterized by TEM. Some images of the results have been shown in a previous work [11]. A complete analysis of the TEM images shown that effectively by controlling germanium interlayer thickness and OPP it is possible to control the deposition of germanium nanoparticles. Figure 5(a) present the results of the grain size distribution and spatial distribution of nanoparticles by area for as function of OPP and Ge intermediate layer thickness. As expected, there is an increase in the density of nanoparticles with increasing roughness accompanied by a decrease in the size. This can be related to an increment in the nucleation sites as roughness increases. To study of dependence with the thickness of the germanium interlayer (d_i) the results of the grain size distribution and spatial distribution of nanoparticles by area of the samples produced employing OPPGe50 (same surface roughness) are presented in Fig. 5b). Here it is observed that as the thickness of the germanium interlayer increases the size of the nanoparticles increases while the number of nanoparticles by area decreases.

As an indirect bandgap material bulk germanium has a low efficiency for radiative recombination but as its dimensions are reduced to nanometers radiative transitions increases due to relaxation in the momentum values available making them quasi-direct transitions. Then it is expected that nanoparticles present a more efficient photoluminescent emission and a shift from the bulk germanium bandgap (0.6 eV) toward higher energies. This effect as function of the oxygen partial pressure employed for the nanoparticles

formation was reported; It was found a blue shift in the energy of the emission band as OPP increases [11]. Figure 6 shows the PLspectra of the samples grown at OPP75 and different thickness for the intermediate layer of germanium: a) ∼2.3 nm, b) ∼4.7 nm and c) ∼7.2 nm. It is worth no remember that germanium nanocrystals produced using OPP75 presented the better crystalline characteristics as shown by XRD. A Gaussian deconvolution of the spectra was performed using just two peaks. As shown in Fig. 6 this approach reproduces the experimental photoluminescence curves. The peak a lowest energy, around 1.4 eV, does not change as germanium nanocrystal size increases then it could be due to the tetragonal phase of germanium. Further research is needed to confirm the origin of this peak but it could be the first experimental report of the bandgap of the germanium tetragonal phase. The broad peak at higher energy has its origin to the contribution of PL emission from germanium nanocrystal with different sizes.

Finally it should be stressed that an important feature of the methodology discussed in this work is that in order to produce the germanium nanoparticles with controlled size distribution it is not necessary to anneal the samples a higher temperatures. The above mentioned results indicate that our methodology reduces the amount of non-radiative traps associated with other procedures.

4. Conclusions

Light emitting Ge-NCs embedded within a SiO_2 matrix were successfully synthesized, using a process which does not require additional post annealing treatment. Atmosphere composition used during deposition by reactive RF sputtering, determine particle size and crystallographic structure of the Ge-NCs and the chemical characteristics of the matrix. Size dispersion tends to decrease for samples grown employing an atmosphere rich in oxygen content producing a stoichiometric SiO_2 matrix. The formation of the tetragonal phase of Ge is promoted by interlayer thickness and the highest crystallographic quality is obtained using high oxygen partial pressure values.

Acknowledgments

The technical support of A. Garcia-Sotelo, M. Guerrero, R. Fragoso, L. Lopez and D. Perez Escamilla is gratefully acknowledged. A. Hernandez-Hernandez expresses his gratitude to UNAM, postdoctoral fellowship DGAPA. This work was partially supported by CONACyT-Mexico and ICyT-DF by project 336/2010. Also, A. Hernandez-Hernandez acknowledge financial support from PRODEP, grant UAEH-PTC-693 DSA/103.5/15/7001. *On sabatical leave from Departamento de Física, Cinvestav-IPN.

1. Teal, G.K. Electron Devices, *IEEE Transactions on*, **23** (1976) 621-639. and references therein
2. P.S. Goley,, & M.K. Hudait, *Materials*, **7** (2014) 2301-2339.
3. G.K. Teal, *IEEE Transactions on electron devices*, **23** (1976) 7.
4. D. Lubyshev *et al*., *Journal of Vacuum Science & Technology B* **26** (2008) 1115.
5. Kim E. Sapsford, *et al*., *Chem. Rev.*, **113** (2013) 1904-2074.
6. Elsa Cassettea *et al*., *Advanced Drug Delivery Reviews* **65** (2013) 719-731.
7. Sanshiro Hanada *et al*., *Int. J. Mol. Sci.* **14** (2013) 1323-1334.
8. Salvatore Cosentino *et al*., *J. Appl. Phys.* **115** (2014) 043103.
9. Sahu *et al*. *Nanoscale Research Letters* **6** (2011) 177.
10. C. Bonafos *et al*., *Materials Science in Semiconductor Processing* **15** (2012) 615-626.
11. A. Hernández-Hernández *et al*., *J. Appl. Phys.* **111** (2012) 044327.
12. Chou *et al*. *Nanoscale Research Letter*, **7** (2012) 291.
13. Zhenrui Yu and Mariano Aceves-Mijares, *Appl. Phys. Lett.* **95** (2009) 081101.
14. Baojie Yan, Jeffrey Yang, and Subhendu Guha, *J. Vac. Sci. Technol. A* **30** (2012) 04D108.
15. A.A. Shklyaev and M. Ichikawa, *Physics-Uspekhi* **51** (2008) 133.
16. M. Roczen *et al*., *Appl Phys A* **108** (2012) 719-726.
17. S. Saeed, C. de Weerd, P. Stallinga, F.C. Spoor, A.J. Houtepen, L.D. Siebbeles, & T. Gregorkiewicz, *Light: Science & Applications* **4** (2015) e251.
18. D. Vasilache, *et al*., *Phys. Status Solidi A.* (2015) doi: 10.1002/pssa.201532376
19. M.T. Yu, K.Y. Chen, Y.H. Chen, C.C. Lin, & Y.H. Wu, *RSC Advances* **5** (2015) 13550-13554.
20. K.U. Joshi, D. Kabiraj, A.M. Narsale, D.K. Avasthi, T.N. Warang, and D.C. Kothari, *Surf. Coat. Technol.* **203** (2009) 2482.
21. M. Buljan *et al*., *Phys. Rev. B* **82** (2010) 125316.
22. A. Hernández-Hernández *et al*., *Solid State Phenomena* **178-179** (2011) 61-66.
23. L.W. Rieth and P.H. Holloway, *Journal of Vacuum Science & Technology A* **22** (2004) 20.
24. I.D. Sharp *et al*., *Journal of Applied Physics* **100** (2006) 114317.

25. I. Stavarache *et al*., *J. Nanopart. Res.* **13** (2011) 221 and references therein.
26. J.D. Joannopoulos and M.L. Cohen, *Phys. Rev. B* **8** (1973) 2733.
27. D. Tomanek and M.A. Schluter, *Phys. Rev. B* **36** (1987) 1208.
28. X.L. Wu, T. Gao, G.G. Siu, S. Tong, X.M. Bao, *Appl. Phys. Lett.* **74** (1999) 2420.
29. P.G. Pai, S.S. Chao, Y. Takagi, and G. Lucovshy, *J. Vac. Sci. Technol. A* **4** (1986) 486.
30. S. Miyazaki, K. Sakamoto, K. Shiba, and M. Hirose, *Thin Solid Films* **255** (1995) 99.
31. I.W. Boyd and J.B.L. Wilson, *J. Appl. Phys.* **53** (1982) 4166.
32. J.-Y. Zhang, X.-M. Bao, and Y.-H. Ye, *Thin Solid Films* **323** (1998) 68.
33. I.P. Lisovskii, V.G. Litovchenko, V.B. Lozinskii, and G.I. Steblovskii, *Thin Solid Films* **213** (1992) 164.
34. A. Lehmann, L. Schumann, and K. Huber, *Phys. Status Solidi B* **117** (1983) 689.
35. I.P. Lisovskii *et al.*, *J. Non-Cryst. Sol.* **187** (1995) 91.
36. G. Perez and J.M. Sanz, *Thin Solid Films* **416** (2002) 24.
37. I.P. Lisovskyy, S.A. Zlobin, É.B. Kaganovich, É.G. Manooelov, E.V. Begun, *Fizika i Tekhnika Poluprovodnikov*, **42** (2008) 560-565.